

Numerical analysis of a multistable capsule system under the delayed feedback control with a constant delay

Zhi Zhang^a, Joseph Páez Chávez^{b,c}, Jan Sieber^a, Yang Liu^{a,*}

^a*Faculty of Environment, Science and Economy, University of Exeter, North Park Road, Exeter EX4 4QF, UK*

^b*Center for Applied Dynamical Systems and Computational Methods (CADSCOM), Faculty of Natural Sciences and Mathematics, Escuela Superior Politécnica del Litoral, P.O. Box 09-01-5863, Guayaquil, Ecuador*

^c*Center for Dynamics, Department of Mathematics, TU Dresden, D-01062 Dresden, Germany*

Abstract

The vibro-impact capsule system is a self-propelled mechanism that has abundant coexisting attractors and moves rectilinearly under periodic excitation when overcoming environmental resistance. In this paper, we study the control of coexisting attractors in this system by using a delayed feedback controller (DFC) with a constant delay. The aim of our control is to steer this complex system toward an attractor with preferable performance characteristics among multiple coexisting attractors, e.g., a periodically fast forward progression. For this purpose, we give an example of a feedback-controlled transition from a period-3 motion with low progression speed to a period-1 motion with high progression speed at the system parameters where both responses coexist. The effectiveness of this controller is investigated numerically by considering its convergence time and the required control energy input to achieve transition. We combine pseudo-spectral approximation of the delay, event detection for the discontinuities and path-following (continuation) techniques for non-smooth delay dynamical systems to carry out bifurcation analysis. We systematically study the dynamical performance of the controlled system when varying its control gain and delay time. Our numerical simulations show the effectiveness of DFC under a wide range of system parameters. We find that the desired period-1 motion is achievable in a range of control delays between a period-doubling and a grazing bifurcation. Therefore, two-parameter continuation of these two bifurcations with respect to the control delay and control gain is conducted to identify the delay-gain parameter region where the period-1 motion is stable. The findings of this work can be used for tuning control parameters in experiments, and similar analysis can be carried out for other non-smooth dynamical systems with a constant delay term.

Keywords: Coexisting attractors; Delay feedback control; Non-smooth dynamical system; Vibro-impact; Numerical continuation

1. Introduction

The vibro-impact capsule system [1, 2] is a typical piecewise-smooth dynamical system, which consists of a periodically excited inner mass interacting with the main body in the presence of environmental resistance for rectilinear progression. The vibro-impacting driven concept has been adopted to design the self-propelled capsule system for active gastrointestinal endoscopy [3]. However, due to its high degree of nonlinearity, the dynamics of the system may witness a significant change when any small variation from the environment or in the system parameter is encountered. For example, in [4], the system has two coexisting attractors near a grazing event with fractal basins of attraction, indicating that a small perturbation on its initial conditions may result in different dynamical responses. In [5], by changing the frequency or the amplitude of excitation slightly, the direction of capsule's drift can be switched,

*Corresponding author. Tel: +44(0)1392-724654, e-mail: y.liu2@exeter.ac.uk.

Email addresses: zz326@exeter.ac.uk (Zhi Zhang), jpaez@espol.edu.ec (Joseph Páez Chávez), j.sieber@exeter.ac.uk (Jan Sieber), y.liu2@exeter.ac.uk (Yang Liu)

if the stiffness ratio of the system is kept at a low value. Because of its complex dynamics and high sensitivity to parameter variation, the dynamics of such vibration-driven capsule systems have received extensive attention from many researchers in the past decade. For example, in [6], Chernousko presented that a two-mass system can be driven by the internal force from interaction between two main bodies, which becomes the basic concept for developing self-driven capsule system. Following this concept, Li *et al.* built a prototype capsule robot driven by a magnet rod and proposed a strategy to achieve the one-dimensional motion [7]. In [8], Gu and Deng found that the random stick-slip phenomena appears in the capsule system with Hertzian contact and random environmental perturbation, and stochastic P-bifurcation may happen by varying the system parameters. On the other hand, Zhao and Ouyang [9] theoretically studied a capsule-structured triboelectric energy harvester and showed that its performance was not limited by its frequency bandwidth, which was different from other types of vibration-based energy harvesters. For these vibration-driven systems, multistability is an intrinsic property associating with the possession of two or more coexisting attractors for a given set of parameters. For example, in [10], a three-degree-of-freedom vibro-impact system coexists tori T^3 attractor and other types of attractors, such as period-3 and tori T^2 near the codimension-3 bifurcation. In [11], Xu and Ji showed that a vibro-impact system coexists stable, and unstable impact motions and the non-impact periodic motion were observed in a small range between the grazing and the saddle-node bifurcations. As a consequence, the capsule system can present different performances based on different attractors. For example, some attractor presents forward or backward progression, while some performs periodic or chaotic motion, under the same values of system parameters [4]. In addition, the coexisting attractors may have different motion efficiencies in terms of energy consumption and progression rate, even that they all present periodic responses with forward progressions. Hence, from a practical point of view, controlling multistability is useful to determine the motion of the capsule system and to improve its working efficiency, in particular for the self-propelled capsule endoscopy in the intestinal environment. To this end, developing a reliable control method for the vibro-impact capsule system is crucial.

From an engineering perspective, there are two major issues related to multistability. On the one hand, the performance of multistable systems can be easily altered without changing their control parameters, e.g., [12, 13]. On the other hand, some of the coexisting attractors of these systems may correspond to the states causing costly failure. In details, for the application of Jeffcott rotor system, at some cases with bistability, grazing-induced chaotic motion treated as undesired motion, and dangerous vibration should be avoided [14]. Hence, it is necessary to control the system to avoid this type of parameter region and ensure systems have high efficient performance. Similar problems can be found in drill-strings system, where the coexisting stick-slip oscillations causing bit wear and inefficient drilling should be avoided [15]. Thus, control of multistability is essential for maintaining system stability while improving its performance. For this reason, it has received considerable attention from the nonlinear dynamics research community in the past few decades, see [16, 17]. Many useful control methods were developed to control the multistability of dynamical system for presenting a desired motion. For example, in [18], the OGY method was proposed to stabilise chaotic attractors to an embedded unstable periodic attractor, which was adopted later for controlling chaos in different dynamical systems [19]. In terms of non-smooth dynamical systems, the OGY method presented good performance in many applications, such as the mass-beam system with an elastic stop [20], the piecewise linear oscillator [21, 22] and the impact-friction oscillator [23]. Besides that, in [17], Pisarchik and Feudel presented an efficient way to control the multistability based on annihilating all undesired coexisting attractors. However, this could result in the alterations of existing structure of dynamical systems, thus the basins of attraction, indicating the original dynamics cannot be preserved by introducing this method. Similar features and control results can be found in bifurcation control methods, see e.g., [24, 25], which focus on controlling the appearance of some bifurcations, such as the pitchfork and the saddle-node bifurcations, to enlarge the stable region of the desired motion or postpone the appearance of the jump and hysteresis phenomena. In order to avoid this problem, some new control methods were developed to not only achieve the control of multistability, but also keep the original dynamics of the controlled system. In [26], a linear gain feedback control based on the feedback of the desired attractor was used to control the coexisting attractors in an impacting system. In [27], a parameter control method was developed to generate a continuous path between the coexisting attractors for a class of non-autonomous dynamical systems. Wang *et al.* [28] applied a

parameter perturbation method to the nonlinear dynamical networks and achieved the switching from one attractor to the desired one. For a similar network, Cornelius *et al.* [29] developed a feedback control method which generates a small perturbation on system state to achieve the switching among coexisting attractors. In [30], a delay feedback control was applied to a soft impact oscillator to control its coexisting attractors near grazing.

Delayed feedback control (DFC). The present work will consider a DFC with Pyragas-type delay feedback control for controlling multistability in a vibro-impact capsule system. DFC is of the form [31]

$$u(t) = K (y(t) - y(t - \tau_d)),$$

where K , τ_d and y are suitably chosen control gain, delay and output of the system, respectively. Vibro-impact capsules pose a number of issues potentially addressable by feedback control, such as choosing between forward or backward motion [4] and the control of multistability [32]. These applications are meaningful, since this control principle can be the potential tool to control the multistability of many different systems based on the concept of vibro-impact capsule system, such as the worm-like robots [33], the deformable robots with a magnetizable material [34], and the two-sided vibro-impact energy harvester [9, 35]. In addition, there are many advantages to applying the DFC for the control of multistability. For example, DFC can make the controlled non-smooth dynamical systems monostable, even at the near-grazing regime, simplifying the complex dynamics while keeping the controlled system stable at the desired motion. Also, compared with the classical PID control method [36] and the parameter control method [27], this method does not need to have the detailed information of the desired attractor and trajectory as the reference signal, but only requires the information of desired period of targeting attractor (set equal to the delay τ_d in the control). DFC is easy to be implemented for complex nonlinear dynamical systems, because it only needs partial information of system states [37, 38], compared with the LQR method which designs the controller for linear systems to minimise a cost function [39]. Unlike traditional vibration control strategies, such as passive [40], active and semi-active control [41], which introduce significant changes to system's structure and keep the controlled system away from its original dynamics, a system with DFC can asymptotically converge to the desired dynamics of the original uncontrolled system. Thus, both benefits motivate us to use the DFC to control the capsule system.

DFC was first introduced by Pyragas [31] to stabilise chaos to an (originally) unstable periodic orbit. When introducing this controller into the vibro-impact capsule system, the finite dimensional non-smooth dynamical system becomes an infinite-dimensional system. Undoubtedly, the combination of this change and the non-smooth properties may induce new difficulties for analysing the time-delayed non-smooth dynamical system [42]. These difficulties may lead the analysis of non-smooth delay differential equations (DDEs) to failure through utilising the existing numerical continuation software packages directly (e.g., DDE-BIFTOOL [43, 44], PDDE-CONT [45] and Knut [46]). Therefore, the path-following analysis based on the approximate numerical approach proposed in [47] will be employed to study the dynamics of the vibro-impact capsule system under the time-delayed feedback control. In addition, in the present work, we will study the effectiveness of the proposed controller with the consideration of some specific performance indices, so optimising both the capsule system and the controller.

The main contribution of the present paper is to employ the DFC with a constant delay to control the motion of the vibro-impact capsule system via controlling its coexisting attractors. To this end, we will adopt a numerical approach based on path-following techniques to analyse the dynamical responses of the capsule system. The rest of the paper is organised as follows. In Section 2, the physical model and equations of motion of the vibro-impact capsule system are introduced, as well as the mathematical formulation of the DFC. In Section 3, bifurcations of the vibro-impact capsule system with power spectrum density are analysed numerically, and the dynamical performance of the controlled system are studied numerically with respect to some specific performance indices, such as the convergence time and the control energy. In Section 4, further numerical bifurcation analysis of the controlled system is carried out by using the path-following (continuation) methods. Finally, conclusions of the present work are given in Section 5.

2. Mathematical model

In this paper, a vibro-impact capsule system depicted in Fig. 1 is considered. This system consists of two parts: an inner actuator and a rigid capsule. In details, the main part of the inner actuator is the internal mass m_1 driven by an external harmonic force with amplitude P_d and frequency Ω , and a weightless plate. This inner mass is connected to the rigid capsule via a linear spring with stiffness k_1 and a viscous damper with damping coefficient c , and the plate is connected with the capsule via a secondary linear spring with stiffness k_2 . The absolute displacements of the internal mass and the capsule denote by X_1 and X_2 , respectively. If $X_1 - X_2 \geq G$, where G is the gap, the weightless plate can be hit by the internal mass m_1 . The capsule starts to move forward or backward until the elastic force acting on the capsule exceeds the threshold of the dry friction force P_f between the capsule and supporting surface. In this study, we use Coulomb friction to calculate the frictional force between the capsule and the supporting surface as

$$f = -\text{sign}(\dot{X}_2) \cdot P_f, \quad \dot{X}_2 \neq 0, \quad (1)$$

and f equals to the net elastic force from the inner mass and is with the opposite direction of this force, if $\dot{X}_2 = 0$, where $P_f = \mu(m_1 + m_2)g$, μ is the friction coefficient between the capsule and the sliding surface, and g is the gravitational acceleration. Thus, the dimensional equation of the motion with a

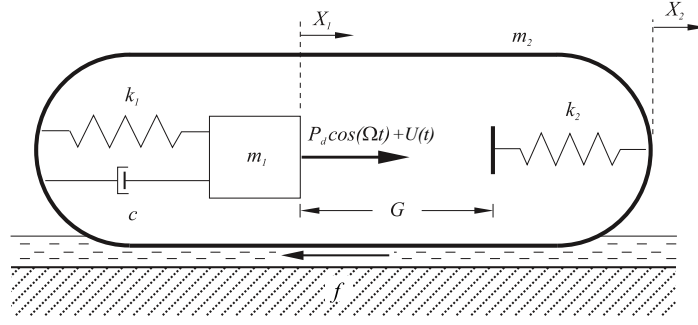


Figure 1: Physical model of the vibro-impact capsule system.

controller $U(t)$ can be constructed as follows [1].

- (i) When the contact between the mass m_1 and the plate does not happen ($X_1 - X_2 < G$) and the capsule m_2 is stationary, the motion of the internal mass m_1 and the capsule m_2 can be expressed as

$$m_1 \ddot{X}_1 = P_d \cos(\Omega t) + U(t) + k_1(X_2 - X_1) + c(\dot{X}_2 - \dot{X}_1), \quad (2)$$

$$\dot{X}_2 = 0, \quad (3)$$

where the threshold of the dry friction force is larger than the net elastic force acting on the capsule, i.e., $|k_1(X_2 - X_1) + c(\dot{X}_2 - \dot{X}_1)| < P_f$.

- (ii) When there is no contact between the mass m_1 and the plate ($X_1 - X_2 < G$) and the capsule is moving, the equation of motion of the internal mass can be expressed as Eq. (2), and the capsule can be written as

$$m_2 \ddot{X}_2 = -\text{sign}(\dot{X}_2) \cdot P_f - k_1(X_2 - X_1) - c(\dot{X}_2 - \dot{X}_1). \quad (4)$$

It is worth noting that the dry friction force acting on the capsule has an opposite direction with the net elastic force acting on the capsule, when the net elastic force just equals to the threshold of the dry friction force, i.e., $|k_1(X_2 - X_1) + c(\dot{X}_2 - \dot{X}_1)| = P_f$, and the capsule begins to move. At

this moment, the dry friction force can be described as

$$f = -\text{sign}(k_1(X_2 - X_1) + c(\dot{X}_2 - \dot{X}_1)) \cdot P_f. \quad (5)$$

- (iii) When the contact between the mass m_1 and the plate occurs ($X_1 - X_2 \geq G$) and the threshold of the dry friction force is larger than the net elastic force acting on the capsule ($|k_1(X_2 - X_1) + c(\dot{X}_2 - \dot{X}_1) - k_2(X_1 - X_2 - G)| < P_f$), the capsule is stationary, and the equations of motion of the internal mass and the capsule can be written as

$$m_1 \ddot{X}_1 = P_d \cos(\Omega t) + U(t) + k_1(X_2 - X_1) + c(\dot{X}_2 - \dot{X}_1) - k_2(X_1 - X_2 - G), \quad (6)$$

$$\dot{X}_2 = 0. \quad (7)$$

- (iv) When there is a contact between the mass m_1 and the plate ($X_1 - X_2 \geq G$) and the capsule is moving, the equation of motion of the internal mass can be written as Eq. (6), and the capsule can be expressed as

$$m_1 \ddot{X}_2 = -\text{sign}(\dot{X}_2) \cdot P_f - k_1(X_2 - X_1) - c(\dot{X}_2 - \dot{X}_1) + k_2(X_1 - X_2 - G). \quad (8)$$

Similarly as phase (ii), the direction of dry friction force acting on the capsule should be opposite to the net elastic force acting on the capsule, when the net elastic force just equals to the threshold of the dry friction force ($|k_1(X_2 - X_1) + c(\dot{X}_2 - \dot{X}_1) - k_2(X_1 - X_2 - G)| = P_f$), and the capsule begins to move. At this moment, the dry friction force can be written as

$$f = -\text{sign}(k_1(X_2 - X_1) + c(\dot{X}_2 - \dot{X}_1) - k_2(X_1 - X_2 - G)) \cdot P_f. \quad (9)$$

To simplify the analysis, the above equations of motion will be transformed into dimensionless form based on the following nondimensional variables

$$\tau = \Omega_0 t, \quad x_i = \frac{k_1}{P_f} X_i, \quad y_i = \frac{dx_i}{d\tau} = \frac{k_1}{\Omega_0 P_f} \dot{X}_i, \quad \dot{y}_i = \frac{dy_i}{d\tau} = \frac{k_1}{\Omega_0^2 P_f} \ddot{X}_i,$$

(for $i = 1, 2$) and parameters

$$\Omega_0 = \sqrt{\frac{k_1}{m_1}}, \quad \omega = \frac{\Omega}{\Omega_0}, \quad \alpha = \frac{P_d}{P_f}, \quad \delta = \frac{k_1}{P_f} G, \quad \beta = \frac{k_2}{k_1}, \quad \zeta = \frac{c}{2m\Omega_0}, \quad \gamma = \frac{m_2}{m_1}.$$

The resulting system variables and parameters are summarised in Table 1.

Table 1: Non-dimensionalised time, state variables and system parameters.

Variable	Value	Description
τ	\mathbb{R}	Time in multiples of natural period $1/\Omega_0$ of internal mass-spring system
x_1, y_1	\mathbb{R}	Displacement, velocity of internal mass
x_2, y_2	\mathbb{R}	Displacement, velocity of capsule shell
Ω_0		Natural frequency of internal mass-spring system
ω	[0.93, 1.03]	Forcing frequency in multiples of natural frequency Ω_0
α	1.6	Forcing amplitude relative in multiples of static friction force P_f
δ	0.02	Gap between plate and internal mass at rest
β	15	Spring stiffness of plate relative to stiffness of internal mass-spring system
ζ	0.01	Relative damping of internal mass-spring system
γ	5	Weight of the rigid capsule relative to the weight of internal mass

The operation of the vibro-impact capsule system with the DFC in different phases can be expressed

as below.

(i) *No contact with stationary capsule: $x_2 - x_1 < \delta$, $y_2 = 0$,*

$$\begin{aligned}\dot{x}_1 &= y_1, \\ \dot{y}_1 &= \alpha \cos(\omega\tau) + (x_2 - x_1) + 2\zeta(y_2 - y_1) + u(\tau), \\ \dot{x}_2 &= 0, \\ \dot{y}_2 &= 0.\end{aligned}\tag{10}$$

(ii) *No contact with moving capsule: $x_2 - x_1 < \delta$, $y_2 < 0$ or $y_2 > 0$,*

$$\begin{aligned}\dot{x}_1 &= y_1, \\ \dot{y}_1 &= \alpha \cos(\omega\tau) + (x_2 - x_1) + 2\zeta(y_2 - y_1) + u(\tau), \\ \dot{x}_2 &= y_2, \\ \dot{y}_2 &= [-\text{sign}(y_2) - (x_2 - x_1) - 2\zeta(y_2 - y_1)]/(\gamma).\end{aligned}\tag{11}$$

(iii) *Contact with stationary capsule: $x_2 - x_1 > \delta$, $y_2 = 0$,*

$$\begin{aligned}\dot{x}_1 &= y_1, \\ \dot{y}_1 &= \alpha \cos(\omega\tau) + (x_2 - x_1) + 2\zeta(y_2 - y_1) - \beta(x_1 - x_2 - \delta) + u(\tau), \\ \dot{x}_2 &= 0, \\ \dot{y}_2 &= 0.\end{aligned}\tag{12}$$

(iv) *Contact with moving capsule: $x_2 - x_1 > \delta$, $y_2 < 0$ or $y_2 > 0$,*

$$\begin{aligned}\dot{x}_1 &= y_1, \\ \dot{y}_1 &= \alpha \cos(\omega\tau) + (x_2 - x_1) + 2\zeta(y_2 - y_1) - \beta(x_1 - x_2 - \delta) + u(\tau), \\ \dot{x}_2 &= y_2, \\ \dot{y}_2 &= [-\text{sign}(y_2) - (x_2 - x_1) - 2\zeta(y_2 - y_1) + \beta(x_1 - x_2 - \delta)]/\gamma.\end{aligned}\tag{13}$$

The resulting vector field governing the motion of x_1, x_2 will be piecewise smooth and the phase space \mathbb{R}^4 for (x_1, y_1, x_2, y_2) will hence be divided into six different regions. A detailed description of the properties of these phases and how to develop the motion of the capsule system can be found in [1]. Then, based on the Filippov convention, the equations of motion for the capsule system with the DFC can be written in a compact form as follows [1].

$$\begin{aligned}\dot{x}_1 &= y_1, \\ \dot{y}_1 &= +(x_2 - x_1) + 2\zeta(y_2 - y_1) - H_3\beta(x_2 - x_1 - \delta) + \alpha \cos(\omega\tau) + u(\tau), \\ \dot{x}_2 &= y_2(H_1(1 - H_3) + H_2H_3), \\ \dot{y}_2 &= (H_1(1 - H_3) + H_2H_3)[- \text{sign}(y_2) - (x_2 - x_1) - 2\zeta(y_2 - y_1) + H_3\beta(x_1 - x_2 - \delta)]/(\gamma),\end{aligned}\tag{14}$$

where $H(\cdot)$ is the Heaviside function and functions H_i ($i = 1, 2, 3$) are defined as

$$\begin{aligned}H_1 &= H(|(x_2 - x_1) + 2\zeta(y_2 - y_1)| - 1), \\ H_2 &= H(|(x_2 - x_1) + 2\zeta(y_2 - y_1) - \beta(x_1 - x_2 - \delta)| - 1), \\ H_3 &= H(x_1 - x_2 - \delta).\end{aligned}$$

In the present work, we will consider the capsule system (14) with the DFC $u(\tau)$ for $\tau \geq 0$, where

$$u(\tau) = K (y_1(\tau - \tau_d) - y_1(\tau)), \quad \tau \geq 0,\tag{15}$$

is the DFC with Pyragas-type delay feedback control form [31]. It should be pointed out that the DFC utilises real-time feedback relying on the velocities of the inner mass at the present time τ and the historical time $\tau - \tau_d$ only. In Eq. (15), the control gain $K \geq 0$ determines the coupling strength between the velocity output $y_1(\tau - \tau_d) - y_1(\tau)$, and the time delay $\tau_d > 0$ is tunable (in contrast to a lag introduced by the control loop, which is assumed to be zero here). By fixing $\tau_d = T := 2\pi/\omega$, our purpose is to control the system to achieve the switching from the other attractors to a coexisting period-1 response. For zero gain, $K = 0$, $u(\tau)$ equals zero such that we have purely harmonic excitation with frequency ω and amplitude α . When the DFC is activated with some suitable $K > 0$, the trajectory of the original motion has a chance to be stable on the desired periodic motion with the period, which equals to the time delay τ_d . After the original trajectory is controlled to the desired attractor, the control signal u becomes very small, and the controlled system reverts to the original system, which does not introduce or generate new attractors. Besides that, the DFC has many other advantages on controlling multistability. The DFC only needs the information of desired period of the targeting attractor, rather than the trajectory of the desired attractor. However, it should be noted that with introducing the DFC, the dimension of the controlled system becomes infinite, leading the dynamics of the controlled system (14) to be more sophisticated for analysis.

3. Numerical investigation of the capsule system under the DFC

In this section, we will numerically study the effectiveness of the DFC on controlling the multistability of the vibro-impact capsule system. Meanwhile, some criterions, such as the energy and convergence time, will be considered in our numerical discussions to evaluate the control effect of the DFC under different values of the control gain. Therefore, we will consider two performance measures, which are the control energy

$$E_u = \int_{\tau_c}^{\tau_f} u^2(\tau) d\tau, \quad (16)$$

where τ_c represents the time at which the control law is activated, while τ_f ($\tau_f > \tau_c$) is a given final time of the simulation, and the convergence time

$$T_{\text{conv}}: \arg \min_{\tau \in [\tau_c, \tau_f]} \left\| [x_1(\tau), y_1(\tau), x_2(\tau), y_2(\tau)]^T - [x_{d,1}(\tau), y_{d,1}(\tau), x_{d,2}(\tau), y_{d,2}(\tau)]^T \right\| = \epsilon_b, \quad (17)$$

where ϵ_b is the threshold distance between the controlled trajectory and the desired attractor that normally should be small, $x_{d,i}$ and $y_{d,i}$, ($i = 1, 2$), denote the displacements and velocities of a desired trajectory. The convergence time T_{conv} defined by Eq. (17) measures the time from switch-on of control to the time when the distance between the controlled system and the desired trajectory reaches zero. The first measure E_u describes the expenditure of energy that is consumed by the DFC $u(\tau)$ over the time interval $[\tau_c, \tau_f]$, where we favor lower values of E_u . For the second measure, the convergence time T_{conv} given by Eq. (17), describes the time it takes to reach the desired attractor, where we also favor lower values of T_{conv} . These two measures will help us evaluate the performance of the DFC (15) for different values of control gain K based on the aspects of energy efficiency and convergence speed and determine an optimal control gain K for controlling multistability.

3.1. Control of multistability

Bifurcation analysis of uncontrolled system for $\omega \in [0.93, 0.98]$. Bifurcation analysis is carried out for the vibro-impact capsule system (14) with $u = 0$, i.e., the vibro-impact system without controller. The results of a parameter sweep are presented in Fig. 2 for varying excitation frequency $\omega \in [0.93, 0.98]$. For excitation frequency ω around and above 1.02, the relevant detailed bifurcation analyses can be found in [4]. To construct the bifurcation diagram, zero initial condition, $(x_1, y_1, x_2, y_2) = (0, 0, 0, 0)$, was firstly used. Then both of backward and forward sweeping of bifurcation parameter ω was locally performed for

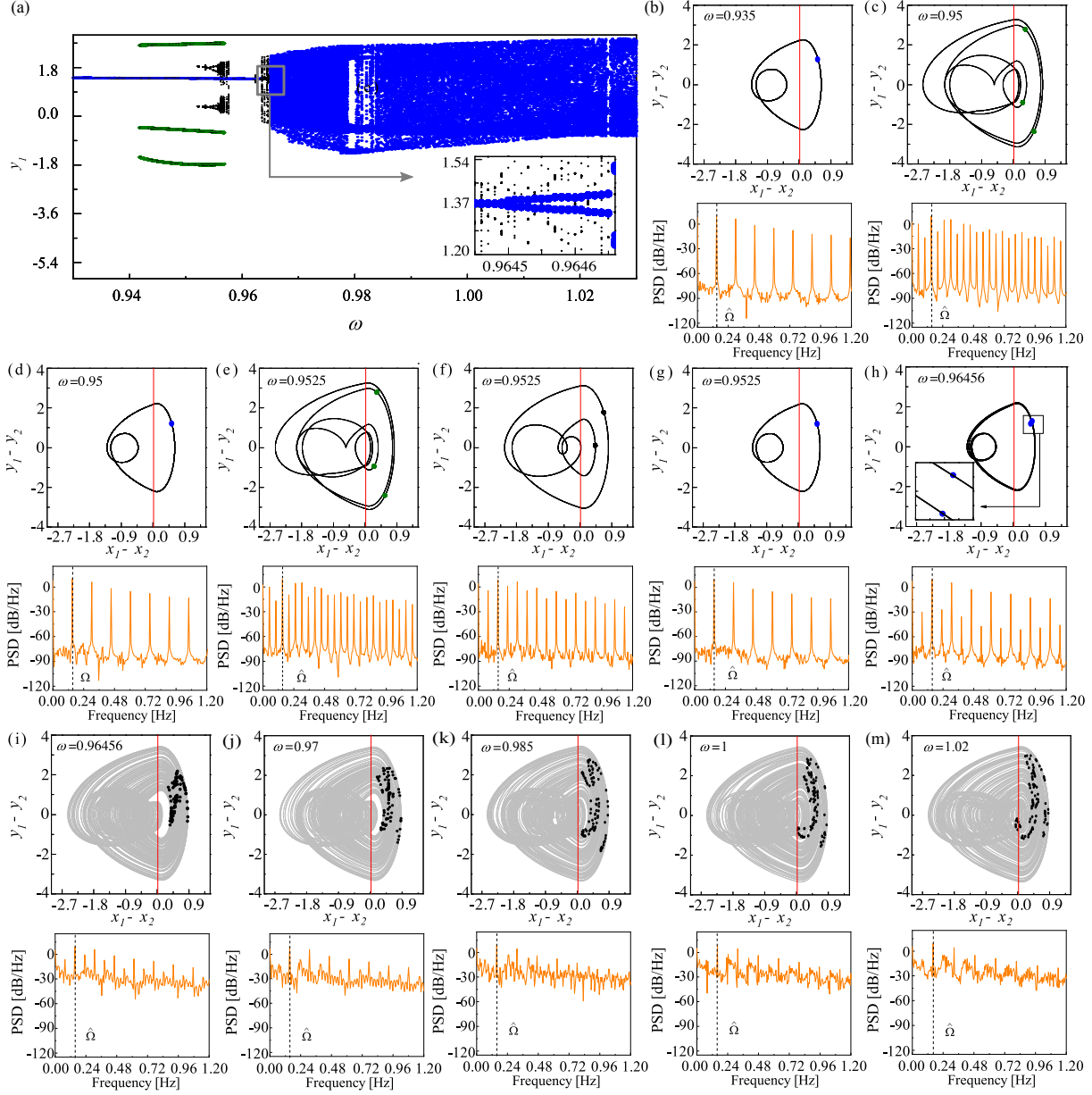


Figure 2: (Colour online) (a) Bifurcation diagram of the vibro-impact capsule system with respect to the excitation frequency ω , computed for $\alpha = 1.6$, $\zeta = 0.01$, $\delta = 0.02$, $\gamma = 5$, $\beta = 15$. Blue, black and green dots denote different coexisting attractors recorded in the computation. Additional panels (b), (c)-(d), (e)-(g), (h)-(i), (j), (k), (l) and (m) present the corresponding attractors at Poincaré sections and their power spectrum densities for $\omega = 0.935, 0.95, 0.9525, 0.96456, 0.97, 0.98, 1$ and 1.02 , respectively. Red vertical and black dash lines indicate the location of the impact boundary and the driven frequency $\hat{\Omega} = \frac{\omega}{2\pi}$, respectively.

coexisting attractors. In the simulation, 350 periods of external excitation were used to obtain each value of the bifurcation parameter ω . The outputs for the first 300 cycles were discarded as transients, whereas the values of velocity of inner mass y_1 at $\tau = \frac{2n\pi}{\omega}$, $n = 301, \dots, 350$ are included in a scatter plot in Fig. 2, generating a bifurcation diagram in the (ω, y_1) -plane. We observe several regions with visibly different qualitative behaviour of system (14) with $u = 0$, and the regularity of typical capsule dynamics can be confirmed by the power spectrum density of capsule's velocity.

- For $\omega \in [0.93, 0.94185]$ the system shows a period-1 motion as the only attractor reached. The top

panel of Fig. 2(b) shows the period-1 trajectory, which is a regular motion with sharp peaks at the driven frequency $\hat{\Omega} = \frac{\omega}{2\pi}$ and its super-harmonics, as shown in the lower panel of Fig. 2 (b).

- For $\omega \in (0.94185, 0.95215]$ two coexisting attractors are found, of which one is the period-1 response (blue) continuing the attractor from smaller ω , and the other is a period-3 (green) response. From the power spectrum density presented in Fig. 2(c) and (d), the period-1 and period-3 responses also have sharp peaks at the driven frequency $\hat{\Omega}$, and their sub- and super-harmonics, with ignorable power.
- For $\omega \in (0.95215, 0.9561]$ three coexisting motions are observed. For example, at $\omega = 0.9525$, the system has a period-1 (blue), a period-3 (green) and a period-2 (black) responses (see Fig. 2(e)-(g)). The period-2 attractor (black in Fig. 2) undergoes a sequence of bifurcations near the large- ω end of this region.
- For $\omega > 0.9561$ the period-3 attractor does not exist anymore. At $\omega \approx 0.96453$, the period-1 response undergoes a period doubling, and then becomes to a period-2 motion. The trajectory of the emerging period-2 response at $\omega = 0.96456$ is shown in Fig. 2(h), and the coexisting chaotic motion is displayed in Fig. 2(i). The range of this period-2 motion is small, giving way to the chaotic motion for $\omega > 0.96469$. The detailed dynamics of this chaotic motion can be seen from Fig. 2(i)-(m), where their power spectrum densities are distributed in a wide frequency region.

Basins of attraction and attractor properties for bistable uncontrolled system at $\omega = 0.95$. As shown in the bifurcation analysis in Fig. 2, the system at $\omega = 0.95$ has two coexisting attractors. The basins of attraction of two coexisting periodic responses are presented in Fig. 3 (a), of which one is the period-3 attractor shown in Fig. 3 (b), and the other one is the period-1 attractor shown in Fig. 3 (c). Figure 3(d,e) show that the average asymptotic progression velocities $\lim_{\tau \rightarrow \infty} (\omega / (2n_p\pi)) \int_{\tau}^{\tau+2n_p\pi/\omega} y_2(s) ds$, $n_p = 1, 3$, of the capsule of these two coexisting motions are different. Specifically, the average velocity of capsule of the period-3 response is 0.0926, but the average velocity of capsule of the period-1 response is 0.1753, which is almost twice that of the period-3 response. Undoubtedly, the capsule presenting the period-1 response progresses further in the same time period and has a faster speed than a capsule showing the period-3 response. Hence, in this scenario, it may be desirable to implement a control u that steers system (14) from its period-3 response with lower average progression speed y_2 to its period-1 response with higher speed.

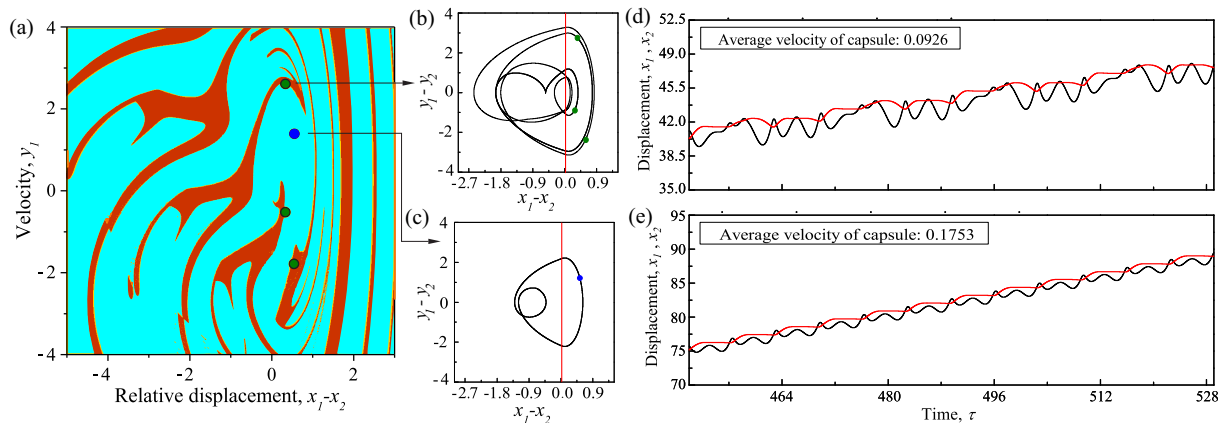


Figure 3: (Colour online) (a) Basins of attraction for the two attractors of the vibro-impact capsule system calculated for $\alpha = 1.6$, $\zeta = 0.01$, $\delta = 0.02$, $\gamma = 5$, $\beta = 15$ and $\omega = 0.95$; (b) period-3 trajectory (green dots with red basin); (c) period-1 trajectory (blue dot with cyan basin), where vertical red lines indicate the location of the impact boundary. (d) Time histories of displacements of the mass, x_1 (black line) and the capsule, x_2 (red line) for the period-3 response. (e) Time histories of displacements of the mass, x_1 (black line) and the capsule, x_2 (red line) for the period-1 response.

Effect of the DFC on the attractors at $\omega = 0.95$. The following analysis studies the DFC (15) for controlling multistability of the vibro-impact capsule system (14). In order to demonstrate the feasibility of the DFC on achieving the above target, we present the bifurcation analysis of the controlled system (14) for varying control gain K in Fig. 4 (a). In Fig. 4 (a), there are 300 cycles of external excitation used to obtain the bifurcation diagram, and only the last 30 values of y_1 were plotted in the bifurcation diagram for each value of the parameter K to ensure the steady state response. Since there are two coexisting periodic responses at $\omega = 0.95$ and among them the period-1 is desired, the DFC (15) with $\tau_d = \frac{2\pi}{\omega}$ was applied to achieve the switching from the period-3 response to the period-1 response. Fig. 4(a) shows that DFC has a large range for the control gain K for which it reaches the control target (the period-1 response) from the period-3 response. When $K \geq 0.0009$, the period-3 response can always be controlled to present period-1 motion. Since the feasible range of the control gain K is large, we have to consider some other performance criteria, such as the energy expenditure E_u , given in (16), and convergence time T_{conv} , given in (17), to determine a suitable value of the control gain K . Fig. 4 (b) and (c) show E_u and T_{conv} for varying control gain K . Initially the energy expenditure E_u stays at a lower level which is smaller than 0.5109, and increase slowly, when $K \in [0.0009, 0.24]$. Then, after 0.24, E_u starts to increase exponentially, which should not be considered as the suitable values for controlling the above multistability scenario. The convergence time T_{conv} , shown in Fig. 4(c) for varying K , has a minimum near $K = 0.11$ ($\min T_{\text{conv}} \approx 551.459$). Since $K = 0.11$ is in the range $[0.0009, 0.24]$, where E_u does not witness significant change, one may consider $K = 0.11$ as the optimal value for control gain K (when weighting the measures E_u and T_{conv} approximately equally).

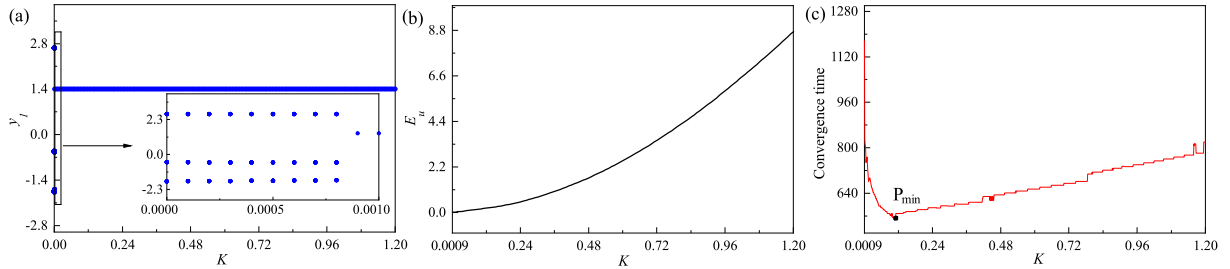


Figure 4: (Colour online) (a) Bifurcation diagram, (b) control energy E_u and (c) convergence time of the vibro-impact capsule system with the DFC, where the control gain K is considered as a branching parameter calculated for $\alpha = 1.6$, $\zeta = 0.01$, $\delta = 0.02$, $\gamma = 5$, $\beta = 15$, $\omega = 0.95$ and $\tau_d = \frac{2\pi}{\omega}$.

Following the above analysis, $K = 0.11$ is chosen as the ideal control gain of the delay feedback control for stabilising the vibro-impact capsule system to the period-1 response. Fig. 5 shows the varying of the mass and capsule position (x_1 and x_2) and the control signal u with respect to the time history. The control gain K was set from 0 to 0.11 after the 81'th period of the excitation, with the effect that the period-3 response was perturbed, steering the system towards the desired period-1 response. Then the system converges to period-1 response at $\tau = 551.459$. The details of the period-1 response can be discovered from the phase plane, as shown in Fig. 5 (a). In addition, the control signal u converges to zero asymptotically, when the control stabilises the vibro-impact capsule system on the period-1 response. Similarly, when $\omega = 1$, the chaotic response can be controlled to the unstable period-1 response by the DFC with the same control gain as shown in Fig. 5 (d-f).

3.2. Variation of the delay

In order to investigate the DFC's performance under the variation of delay time τ_d , we will introduce two measures below. The first one is the *Maximum Velocity Difference* given as

$$\text{mvd}(T, \tau_d) := \max_{\tau > \tau_{\text{stab}}} |y_1(\tau - T) - y_1(\tau)|, \quad (18)$$

where τ_{stab} denotes the time when transient response terminates, and $T = 2\pi/\omega$ is one period of the driving excitation. The second measure is a quantitative characterisation of the invasiveness of the

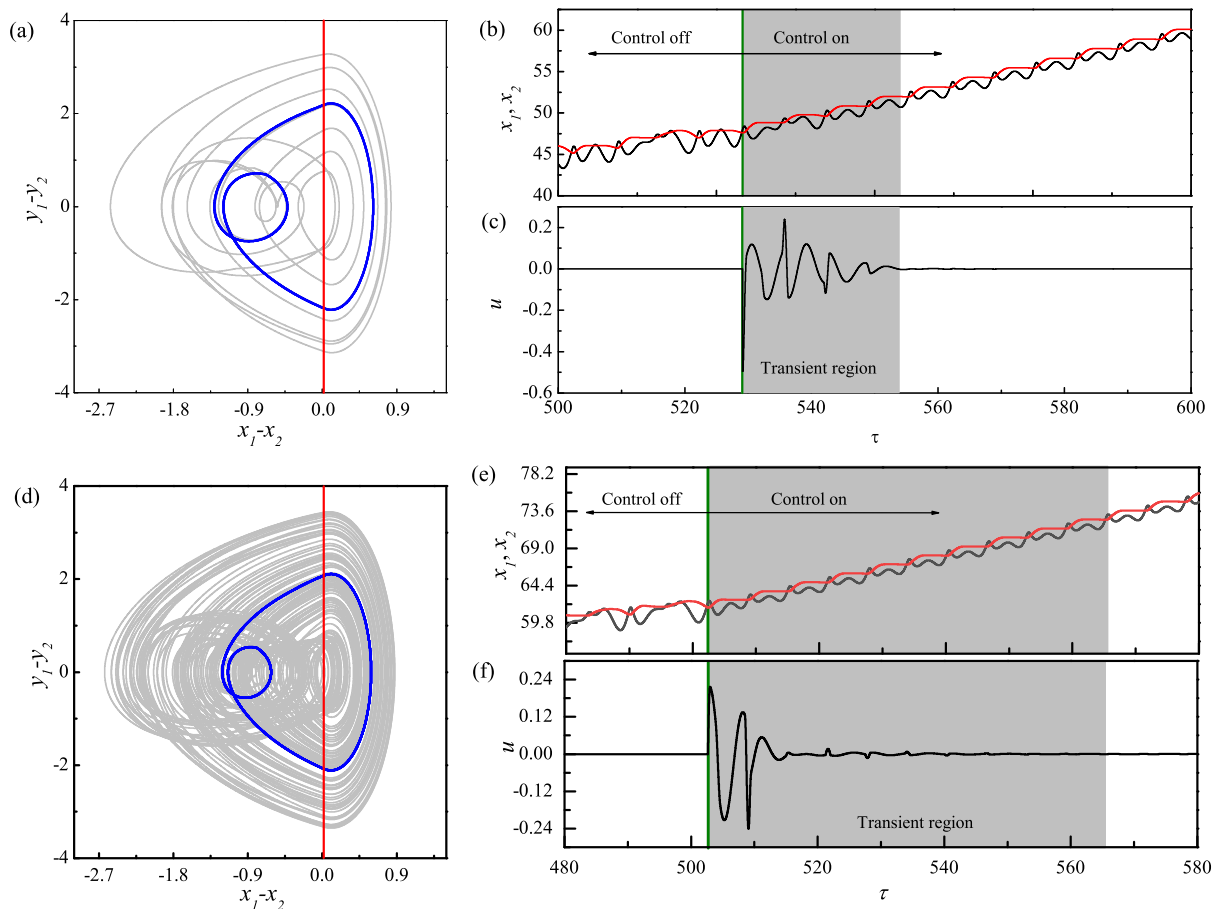


Figure 5: (Colour online) (a) Phase trajectory, (b) displacement and (c) control signal of the period-3 motion before and after the DFC is switched on, computed for $\alpha = 1.6$, $\zeta = 0.01$, $\delta = 0.02$, $\gamma = 5$, $\beta = 15$, $\tau_d = \frac{2\pi}{\omega}$, $K = 0.11$, and $\omega = 0.95$. (d) Phase trajectory, (e) displacement and (f) control signal of the chaotic motion before and after the DFC is switched on, computed for $\alpha = 1.6$, $\zeta = 0.01$, $\delta = 0.02$, $\gamma = 5$, $\beta = 15$, $\tau_d = \frac{2\pi}{\omega}$, $K = 0.11$, and $\omega = 1$. Grey and blue trajectories are without and with the control, red and green vertical lines denote the impact boundary and the time that control is applied, respectively, and grey box indicates the transient region of the controlled system.

DFC [48] written as

$$q_c(\tau_d, K) := \lim_{\delta\tau \rightarrow +\infty} \frac{1}{\delta\tau} \int_{\tau_c}^{\tau_c + \delta\tau} K^2 \langle y_1(\tau - \tau_d) - y_1(\tau), y_1(\tau - \tau_d) - y_1(\tau) \rangle d\tau. \quad (19)$$

In our simulation, we chose τ_{stab} as the 100th period of the external excitation after the control gain K was increased from 0. In our observation the transients of the controlled system have already decayed after this time. When the measure $\text{mvd}(T, \tau_d)$ is zero, the feedback control with delay time τ_d asymptotically (after τ_{stab}) achieves the period-1 response. The measure q_c in (19) presents the average power used to control the capsule system over a certain delay time τ_d .

Our main purpose in this section is to study how the delay time τ_d in the DFC (15) affects the measures $\text{mvd}(T, \tau_d)$ and q_c for the controlled system (14). Fig. 6 shows the dynamic response of system (14) for a parameter sweep of the delay time τ_d . The measure $\text{mvd}(T, \tau_d)$ in (18) shows that there are many delay times $\tau_d \in [0, T]$ for which system (14) reaches a period-1 response from the period-3 response, such as $\tau_d = 0.068T$, $\tau_d = 0.3175T$, $\tau_d = 0.8316T$ and $\tau_d = T$ as shown in Fig. 6 (c) and (g-i), where all the periodic motions have sharp peaks at the driven frequency and their sub- and super-harmonics. Some chaotic responses were also observed at some values of the delay time τ_d , such as $\tau_d = 0.0227T$ and

$\tau_d = 0.0832T$ as shown in Fig. 6 (a) and (e), at where distribute their energies in a wide frequency region and present irregular dynamics.

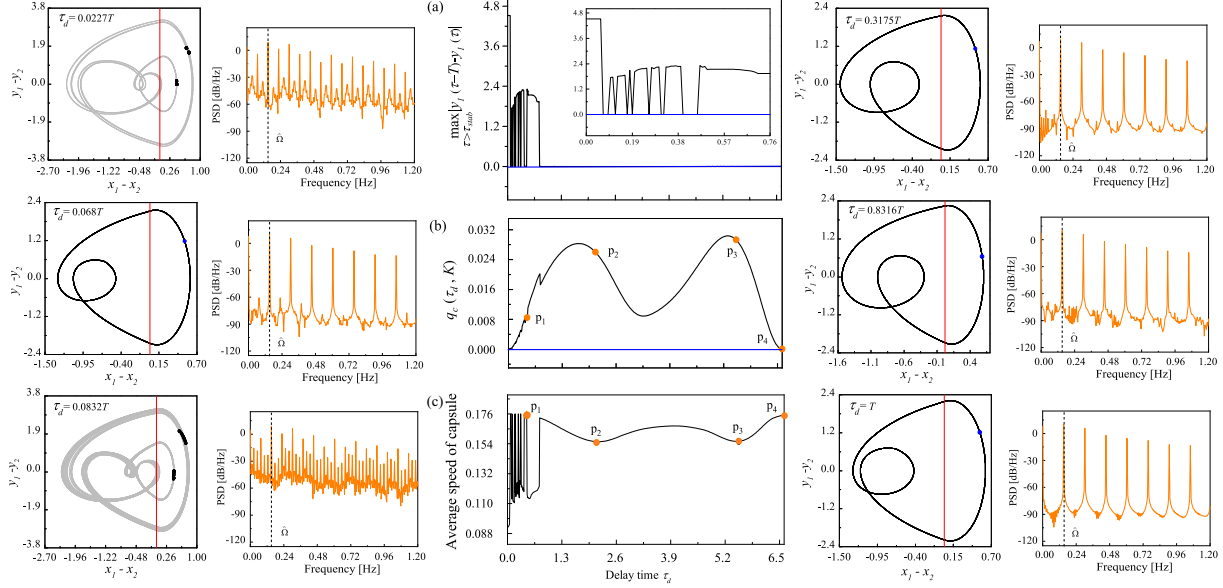


Figure 6: (Colour online) (a) Variation of the maximum absolute difference between $y_1(\tau - T)$ and $y_1(\tau)$, (b) the measure q_c in Eq. (19) and (c) the average velocity of the capsule system as functions of the delayed time τ_d , computed for $\alpha = 1.6$, $\zeta = 0.01$, $\delta = 0.02$, $\gamma = 5$, $\beta = 15$, $\omega = 0.95$, $K = 0.11$ and $T = \frac{2\pi}{\omega}$, where p_1 , p_2 , p_3 and p_4 represent typical period-1 responses for $\tau_d = 0.068T$, $\tau_d = 0.3175T$, $\tau_d = 0.8316T$ and $\tau_d = T$, respectively. Additional panels demonstrate phase trajectories and power spectrum densities of the system recorded for $\tau_d = 0.0227T$ (chaotic), $\tau_d = 0.068T$ (period-1), $\tau_d = 0.0832T$ (chaotic), $\tau_d = 0.3175T$ (period-1), $\tau_d = 0.8316T$ (period-1) and $\tau_d = T$ (period-1). Blue horizontal lines indicate zero value, red vertical lines denote the location of the impact boundary, and vertical dash lines indicate the driven frequency $\hat{\Omega} = \frac{\omega}{2\pi}$.

The measure q_c in Eq. (19) quantifies the control performance of the DFC with respect to the delay time τ_d . As a detailed study was carried out by Páez Chávez et al. [5], we will not study progression optimisation for the capsule system in the present work. As shown in Fig. 6(a) and (b), the relevant $q_c(\tau_d, K)$ at p_1 ($\tau_d = 0.068T$), p_2 ($\tau_d = 0.3175T$), p_3 ($\tau_d = 0.8316T$) and p_4 ($\tau_d = T$) are 0.0085, 0.026, 0.0293 and 9.438×10^{-5} , respectively. It should be pointed out that, among these delay times, $q_c(\tau_d, K)$ at $\tau_d = 0.068T$ is the lowest except for $\tau_d = T$, and the relevant DFC at this delay time can stabilise the system at the period-1 response. On the other hand, the average speed of the capsule at p_1 is also the fastest around 0.175 as shown in Fig. 6(c), and the rest, p_2 , p_3 and p_4 all present high efficient progression speeds. In fact, it is well-known that the dimension of the time-delayed system will be increased with the increasing delay time in the delayed arguments on the right hand side, such that the analysis of the dynamical properties becomes more complex. However, the above analysis shows that DFC (15) with a small delay time τ_d is able to stabilise the capsule system on a period-1 response using a small cost of input while keeping high efficient progression speed. Then system (14) has a low dimension for small τ_d , allowing us to carry out a more detailed bifurcation analysis by using the numerical continuation techniques in the next section.

4. Numerical continuation study of the capsule system with the DFC

This section will investigate the periodic response of the capsule model using numerical continuation methods, taking into account the time-delayed feedback controller described in previous sections. As pointed out before, the main challenge in this study is the fact that, to the best of our knowledge, there is at the moment no specialized software package for numerical continuation of piecewise-smooth delay differential equations. For this reason, the path-following analysis to be presented in this section will be

implemented using the approximate numerical approach proposed in [47], which will be briefly introduced below.

4.1. Approximate equations for numerical continuation of piecewise-smooth DDEs

The numerical framework for the path-following analysis of the capsule system under the DFC is based on the *chain method* [49], improved by a higher-order approximation scheme using a finite sequence of Taylor expansions as follows. Consider a system of delay differential equations (DDEs) with constant delay $\tau_d > 0$

$$\dot{q}(\tau) = f(\tau, q(\tau), q(\tau - \tau_d)), \quad (20)$$

where $f : \mathbb{R} \times \mathbb{R}^d \times \mathbb{R}^d \rightarrow \mathbb{R}^d$ is sufficiently smooth. Choose an $N \in \mathbb{N}$ suitably large and introduce the grid points $\tau_i := i \frac{\tau_d}{N}$, $i = 0, \dots, N$. Furthermore, define the finite sequence of functions $v_i(\tau) := q(\tau - \tau_i)$ for all $\tau \geq 0$, $i = 0, \dots, N$. In this setting, via an M th-order Taylor expansion we obtain

$$v_{i-1}(\tau) = q\left(\tau - \left(\tau_i - \frac{\tau_d}{N}\right)\right) = v_i\left(\tau + \frac{\tau_d}{N}\right) = \sum_{k=0}^M \frac{1}{k!} v_i^{(k)}(\tau) \left(\frac{\tau_d}{N}\right)^k + \mathcal{O}\left(\left(\frac{\tau_d}{N}\right)^{M+1}\right), \quad \text{and} \quad (21)$$

$$\dot{v}_0(\tau) = f(\tau, v_0(\tau), v_N(\tau)), \quad (22)$$

with $\tau \geq 0$, $i = 1, \dots, N$ and $M \geq 1$. Upon neglecting the \mathcal{O} -terms, a system of dN differential equations of order M is derived from (21). This allows us to approximate a piecewise-smooth dynamical system of dimension d with constant delay via a piecewise-smooth system of first-order ODEs of dimension $d(NM+1)$ for large N . In this way, the resulting model can be studied in the context of hybrid dynamical systems [50].

4.2. Mathematical formulation of the time-delayed capsule system for path-following analysis

Let us choose $M = 2$ in the approximation scheme introduced before and denote by $z = (x_r, v_r, r, s, v_0, \dots, v_N, w_1, \dots, w_N)^T \in \mathbb{R}^{2N+5}$ and $\lambda = (\omega, \alpha, \zeta, \delta, \gamma, \beta, K, \tau_d) \in (\mathbb{R}_0^+)^8$ the state variables and parameters of the system, respectively. We consider the coordinate transformation $x_r = x_1 - x_2$, $v_r = y_1 - y_2$, $v_0 = y_1$. In this setting, an approximation of the capsule model with the DFC via a system of piecewise-smooth ODEs is given by

$$\begin{aligned} \dot{z} &= \begin{pmatrix} \tau_d v_r \\ \tau_d \left(\alpha s + \bar{u} - x_r - 2\zeta v_r - H_{k_2} \beta(x_r - \delta) - |H_{\text{vel}}| (x_r + 2\zeta v_r + H_{k_2} \beta(x_r - \delta) - H_{\text{vel}}) / \gamma \right) \\ r + \omega \tau_d s - r (r^2 + s^2) \\ s - \omega \tau_d r - s (r^2 + s^2) \\ \tau_d (\alpha s + \bar{u} - x_r - 2\zeta v_r - H_{k_2} \beta(x_r - \delta)) \\ (w_i)_{i=1, \dots, N} \\ \left(2N^2 \left(v_{i-1} - v_i - \frac{1}{N} w_i \right) \right)_{i=1, \dots, N} \end{pmatrix} \\ &= f_{\text{CAP}}(z, \lambda, H_{k_2}, H_{\text{vel}}), \end{aligned} \quad (23)$$

where w_i are auxiliary variables representing the first derivative of v_i , $1 \leq i \leq N$, and $\bar{u}(\tau) = K(v_N(\tau) - v_0(\tau))$, $\tau \geq 0$, stands for the approximate delay feedback control signal. Notice that a time re-scaling $\tau \leftarrow \tau / \tau_d$ has been adopted in the approximating system (23). In this way, the approximation of the history $q(\tau - t)$ for $t \in [0, \tau_d]$ given by the Taylor expansion (21) is restricted to the unit interval, for any delay τ_d . Moreover, for the approximating system (23) one has that $v_0(\tau) = y_1(\tau)$ and

$$v_i(\tau) \approx y_1(\tau - \tau_i), \quad \text{for all } \tau \geq 0, \quad \tau_i = \frac{i}{N}, \quad i = 1, \dots, N. \quad (24)$$

The approximation scheme introduced here can be considered as a special case of the pseudo-spectral approximation of DDEs by ODEs proposed in [51]. Nevertheless, this spectral approximation presents no advantage over the low-order approximation (24), since the history segment is only differentiable once with Lipschitz continuous derivative whenever a discontinuity boundary (i.e. impact with the secondary spring k_2 , transition from forward to backward capsule motion and so on) is crossed, and therefore the second-order approximation introduced in the present work has the most suitable order M .

Moreover, note that the state variables in the formulation above do not include a coordinate for the capsule position. This information, however, can be recovered from model (23) as follows:

$$x_c(\tau) := x_c^* + \int_0^\tau (v_0(s) - v_r(s)) ds,$$

where $x_c^* \in \mathbb{R}$ represents the position of the capsule (coordinate x_2 in the original model) at $\tau = 0$.

On the other hand, the symbols H_{k_2} and H_{vel} appearing in the approximate system (23) are discrete variables defining the operation modes of the system, according to the rules:

$$H_{k_2}(x_r) = \begin{cases} 1, & x_r - \delta \geq 0, \quad (\text{contact with secondary spring } k_2), \\ 0, & x_r - \delta < 0, \quad (\text{no contact}), \end{cases} \quad (25)$$

$$H_{\text{vel}}(v_c, f_{\text{mc}}) = \begin{cases} 0, & v_c = 0 \text{ and } |f_{\text{mc}}| \leq 1, \quad (\text{capsule stationary}), \\ 1, & v_c > 0 \text{ or } (v_c = 0 \text{ and } f_{\text{mc}} > 1), \quad (\text{forward motion}), \\ -1, & v_c < 0 \text{ or } (v_c = 0 \text{ and } f_{\text{mc}} < -1), \quad (\text{backward motion}), \end{cases} \quad (26)$$

where

$$\begin{aligned} v_c &= y_1 - v_r && (\text{capsule velocity } y_2 \text{ in the original model}), \text{ and} \\ f_{\text{mc}} &= x_r + 2\zeta v_r + H_{k_2}\beta(x_r - \delta) && (\text{force acting on the capsule from the internal mass}). \end{aligned}$$

Therefore, the capsule changes between stationary and forward (backward) motion, whenever the force f_{mc} becomes greater than 1 (or smaller than -1). For the numerical implementation, the discrete variables defined in (25)–(26) will be used to identify the specific operation mode of the capsule. Every operation mode will be associated to a pair $\{\Sigma, \Delta\}$, where $\Sigma \in \{\text{NC}, \text{Ck2}\}$ (no contact or contact with secondary spring k_2 , respectively) and $\Delta \in \{\text{Vc0}, \text{Vcp}, \text{Vcn}\}$ (capsule stationary, forward motion, backward motion). For instance, the operation mode $\{\text{Ck2}, \text{Vcp}\}$ means that the capsule is moving forward with the internal mass in contact with the spring k_2 and so on. In this way, the capsule system can operate under 6 different modes, as listed in Table 2.

Table 2: Operation modes of the capsule system and the corresponding values of the discrete variables H_{k_2} and H_{vel} defined in (25)–(26).

Operation mode	Description	H_{k_2}	H_{vel}
{NC, Vc0}	No contact with k_2 , capsule stationary	0	0
{NC, Vcp}	No contact with k_2 , forward motion	0	1
{NC, Vcn}	No contact with k_2 , backward motion	0	-1
{Ck2, Vc0}	Contact with k_2 , capsule stationary	1	0
{Ck2, Vcp}	Contact with k_2 , forward motion	1	1
{Ck2, Vcn}	Contact with k_2 , backward motion	1	-1

4.3. Continuation of periodic orbits

In this section, a numerical continuation study of the delayed capsule model will be carried out using the approximating system (23) (with $N = 30$), implemented in the continuation platform COCO [52]. For this purpose, the COCO-toolbox ‘hspo’ will be extensively used, which implements a segment-specific discretization strategy in the framework of multisegment boundary-value problems, suitable for numerical continuation and bifurcation detection of periodic solutions of piecewise-smooth dynamical systems. On the other hand, all numerical simulations obtained via direct numerical integration will be generated from the original DDE model (14) using the MATLAB solver ‘dde23’, in combination with its built-in event location routines [53, 54]. In this way, we will be able to detect accurately collisions with the system’s discontinuity boundaries (e.g. impact with the secondary spring k_2 , transition from forward to backward capsule motion and so on).

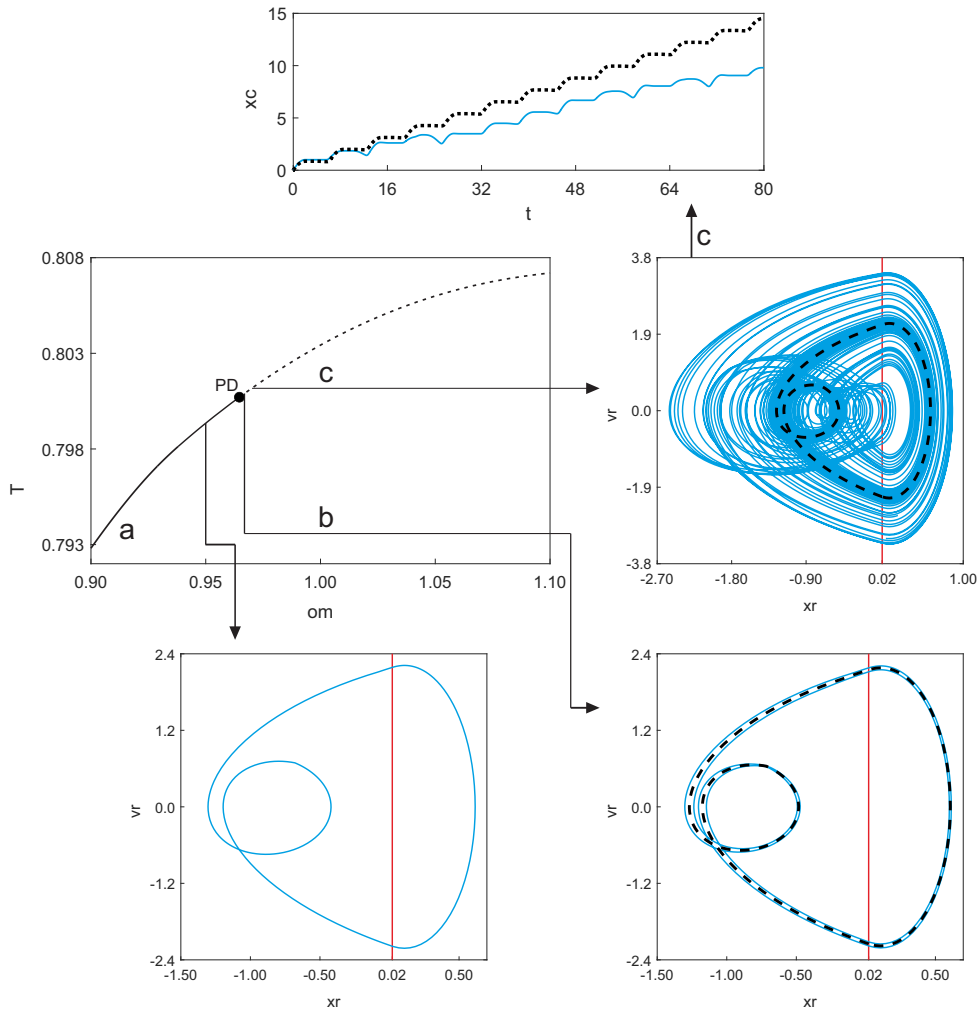


Figure 7: Numerical continuation of period-1 orbits of the capsule system (14) with respect to the excitation frequency ω , with $u = 0$ (i.e. without delay control), and for the parameter values $\alpha = 1.6$, $\zeta = 0.01$, $\delta = 0.02$, $\gamma = 5$, $\beta = 15$. The vertical axis presents the time the oscillating mass is in contact with the secondary spring k_2 . The label PD stands for a period-doubling bifurcation of limit cycles detected at $\omega \approx 0.96453$. Branches of stable and unstable solutions are marked by solid and dashed lines, respectively. Lateral and lower panels depict phase plots corresponding to the test points shown in the bifurcation diagram. The location of the impact boundary $x_r = \delta$ is represented by a vertical red line in the phase plots. For $\omega = 0.96471$ and $\omega = 0.97$ two solutions coexist, one stable (in blue, solid line) and one unstable (in black, dashed curve). The upper panel displays the time plot of the capsule motion for the two coexisting solutions at $\omega = 0.97$.

Let us begin our study with the investigation of the capsule system without control. Specifically, we

will carry out the numerical continuation of the period-1 motion of the capsule model with respect to the frequency of external excitation ω with $K = 0$, for the parameter range displayed in the boxed area of Fig. 2(a). The outcome of the continuation process is shown in Fig. 7. This figure presents the periodic response of the uncontrolled capsule system as ω is varied, with the vertical axis showing the contact time, i.e., the time the oscillating mass is in contact with the secondary spring k_2 . As can be observed in the bifurcation diagram, small values of excitation frequency ω produce stable period-1 solutions (as depicted in the bottom left panel), represented by the solid branch shown in the figure. By increasing ω , a critical point is found, corresponding to a period-doubling bifurcation (labeled PD) of limit cycles. Here, the stability of the period-1 solution is lost, giving rise to a family of stable period-2 solutions, as shown in the bottom right panel of Fig. 7. This panel displays two coexisting solutions for $\omega = 0.96471$, a stable period-2 orbit (in solid blue) produced by the PD point and an unstable period-1 solution (dashed black).

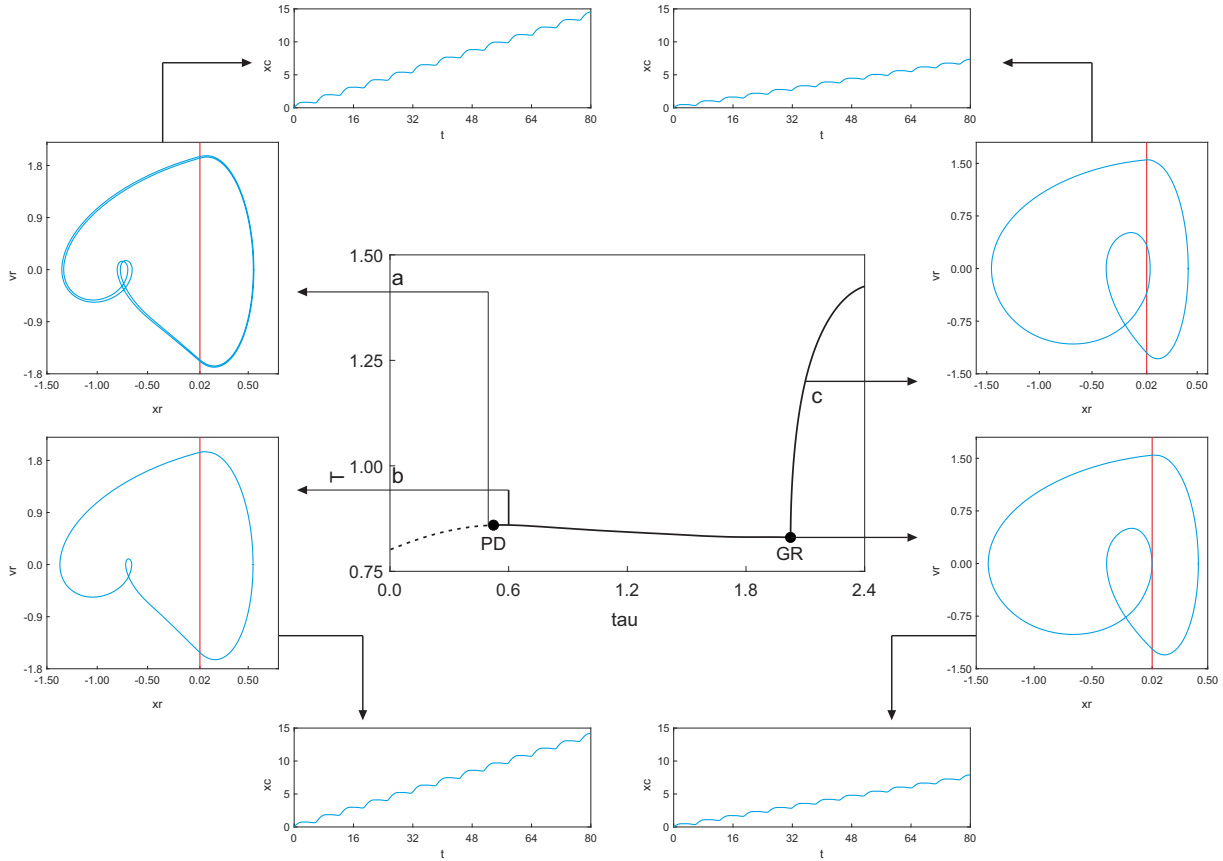


Figure 8: Numerical continuation of periodic orbits of the capsule system (23) (considering time-delayed feedback control) with respect to the control delay τ_d , considering the parameter values given in Fig. 7 (with $K = 0.5$ and $\omega = 0.97$). The vertical axis presents the time the oscillating mass is in contact with the secondary spring k_2 . The labels PD and GR mark period-doubling and grazing bifurcations of limit cycles, located at $\tau_d = \tau_d^{\text{GR}} \approx 0.52329$ and $\tau_d \approx 2.02531$, respectively. The panels displayed on the sides show phase portraits and time plots of the capsule displacement for selected values of the control delay τ_d .

Let us suppose, for instance, that for practical reasons a higher operation frequency is required, for example $\omega = 0.97$, a value not so far away from the period-doubling bifurcation detected above. At this frequency, the system presents a chaotic behaviour as shown in the center right panel depicted in Fig. 7, possibly originating from a period-doubling cascade. As can be seen in this phase plot, the stable chaotic response (in solid blue) coexists with the original unstable period-1 solution (dashed black). From a practical point of view, however, a period-1 behaviour is in general more convenient, for instance due to a better performance in terms of average speed of progression, as can be seen in the time plot

displayed in the upper panel in Fig. 7, showing the capsule motion for the two coexisting solutions at $\omega = 0.97$. Therefore, one of the main questions in the present is how to suitably employ the DFC to stabilize this unstable period-1 response. We will now employ the numerical continuation platform

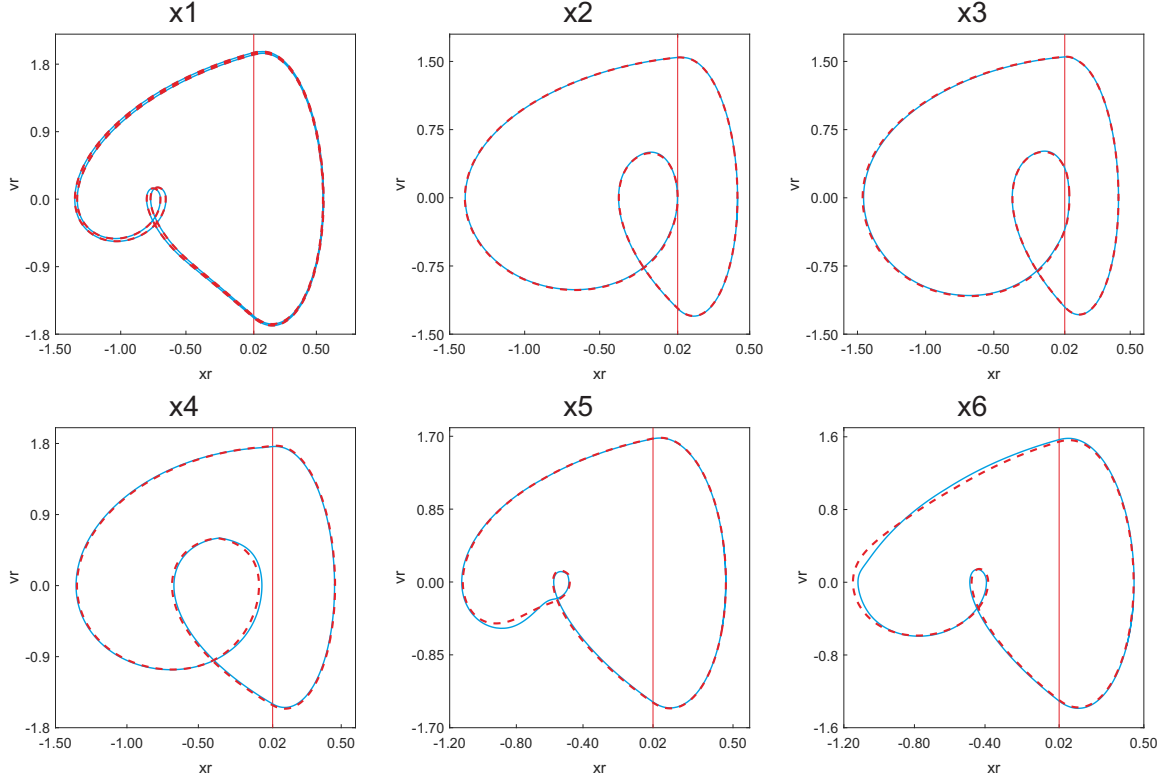


Figure 9: Numerical comparison of the dynamical response of the piecewise-smooth DDE (14) with the approximating system of ODEs (23). The first row shows the phase plots of the solutions obtained in Fig. 8. The lower row displays orbits for higher values of the delay τ_d . The solutions to the original system (14) and their approximations are depicted in blue (solid line) and in red (dashed line), respectively.

COCO to investigate the periodic response of the capsule system (with the DFC) using the approximating system (23). Specifically, we will carry out the numerical continuation of the unstable period-1 solution discussed above with respect to the control delay τ_d . The result is shown in Fig. 8. As expected, a branch of unstable period-1 solutions is found for low values of τ_d . With appearing of period-doubling bifurcation at $\tau_d \approx 0.52329$, this solution becomes stable. As a consequence, the DFC successfully introduces the unstable desired period-1 response into the vibro-impact capsule system and ensures the system being stabilised on period-1 motion by inducing the period-doubling bifurcation. Upper and lower left panels present phase plots computed at test points $\tau_d = 0.52$ and $\tau_d = 0.6$ (before and after the bifurcation), showing stable period-2 and period-1 orbits, respectively. As the time delay increases, a grazing bifurcation (GR) is found at $\tau_d \approx 2.02531$, where a segment of the periodic solution intersects tangentially the impact boundary $x_r = \delta$. This grazing solution is plotted in the bottom right panel shown in Fig. 8, while the upper right panel shows a period-1 solution right after the grazing bifurcation GR. According to these observations, the detected GR point defines a boundary between two operation regimes: period-1 behaviour with one impact with the secondary spring k_2 per excitation period and period-1 solutions with two impacts per period. Therefore, our numerical investigation reveals that the time-delayed feedback control considered in this work has a direct effect on both the stability the desired period-1 motion and impacting regimes in the system.

In order to test the reliability of the approximation scheme (23) employed for the numerical continuation process described above, we will carry out a numerical comparison of the dynamical behaviour of the original piecewise-smooth DDE (14) with that of the approximating system of ODEs (23), for different

values of the delay parameter τ_d , see Fig. 9. In this diagram we present a series of orbits calculated from the original piecewise-smooth DDE using the MATLAB solver ‘dde23’ (solid blue line) together with the approximating solutions obtained from the discretization scheme (23) (dashed red line). For the range considered in the continuation study presented in Fig. 8 we can verify that the computed solutions of the original DDE and those of the approximating ODE system are very close to each other, for different values of τ_d , see first row of Fig. 9. As the time delay increases, however, it can be observed that the dynamical response of the discretization scheme deviates from the solutions of the original system, owing to the truncation error (i.e. the \mathcal{O} -term) neglected from the Taylor expansion (21). For this reason the numerical approach proposed here is unable to provide reliable approximations for arbitrary delays, and hence our study is restricted to small values of τ_d .

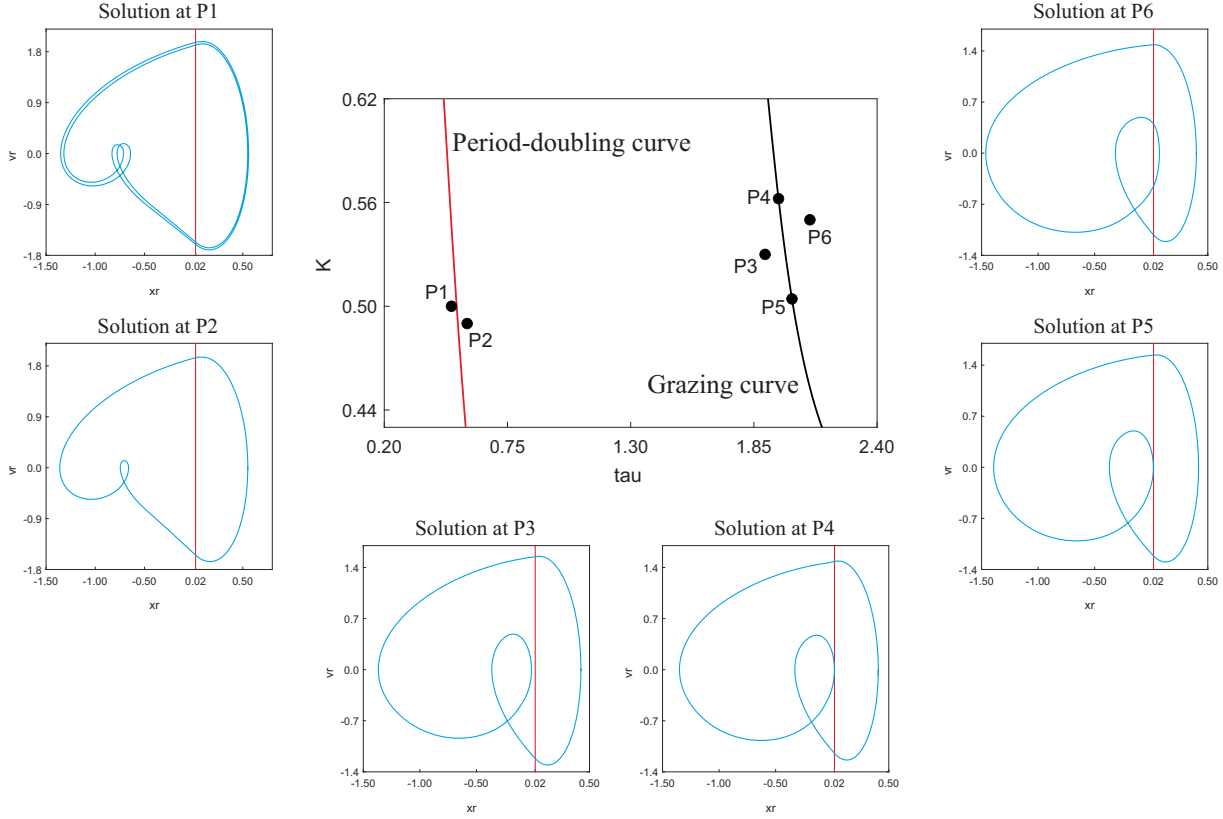


Figure 10: Two-parameter continuation of the period-doubling and grazing bifurcations detected in Fig. 8, with respect to the control parameters τ_d and K . Lateral and lower panels display phase plots corresponding to the test points P1 ($\tau_d = 0.5$, $K = 0.5$), P2 ($\tau_d = 0.57$, $K = 0.49$), P3 ($\tau_d = 1.9$, $K = 0.53$), P4 ($\tau_d = 1.96$, $K \approx 0.56223$), P5 ($\tau_d = 2.02$, $K \approx 0.50423$) and P6 ($\tau_d = 2.1$, $K = 0.55$).

Next, we will investigate the behaviour of the codimension-1 bifurcations discussed above when two control parameters are perturbed, namely, the control delay τ_d and the control gain K . In particular, a locus of grazing periodic orbits will be computed by introducing an extra solution segment with a terminal point satisfying the condition $\dot{x}_r = 0$, where the relative mass velocity becomes zero. In this way, a grazing solution can be detected via the auxiliary boundary condition $x_r - \delta = 0$, and therefore a locus of such orbits can be obtained by freeing two parameters during the continuation process, using the COCO-command ‘coco_xchg_pars’ [52].

In Fig. 10 we present the resulting red and black curves corresponding to the two-parameter continuation of the period-doubling and grazing bifurcations detected in Fig. 8, respectively. In this way, the two-dimensional parameter space is locally divided into three regions. The first region, located to left of the period-doubling curve, gives combinations of τ_d and K yielding unstable period-1 response in the controlled system, and hence stable solutions of higher period or even chaotic behaviour appear in

the system. A supercritical period-doubling bifurcation is produced upon crossing this red line from the right, thereby creating stable period-2 solutions, see for instance the one depicted in Fig. 10 (upper left panel), computed for the test point P1 ($\tau_d = 0.5$, $K = 0.5$). Between the period-doubling and grazing curves a second region is defined, which corresponds to parameter values producing a stable period-1 response with one impact with the secondary spring k_2 per excitation period, as can be seen in Fig. 10 for the test points P2 ($\tau_d = 0.57$, $K = 0.49$) and P3 ($\tau_d = 1.9$, $K = 0.53$). Finally, a third region (to the right of the grazing curve) gives (τ_d, K) pairs producing stable period-1 solutions with two impacts per period, see for instance the test orbit calculated for P6 ($\tau_d = 2.1$, $K = 0.55$) which crosses the impact boundary $x_r = \delta$ with $v_r > 0$ twice. The phase plots computed for P4 ($\tau_d = 1.96$, $K \approx 0.56223$) and P5 ($\tau_d = 2.02$, $K \approx 0.50423$) are calculated on the critical boundary defined by the grazing bifurcation curve (in black), showing solutions making tangential contact with the discontinuity boundary $x_r = \delta$.

5. Conclusions

In this paper, the DFC with a constant delay was considered to control the multistability in a periodically forced capsule system. The control aim was to improve the progression efficiency of the capsule through switching the system to one of its coexisting attractors with the highest progression speed. The performance of the DFC was studied numerically by considering the energy consumption from the control signal and the convergence time to the desired response. In addition, the complex dynamics of the controlled vibro-impact capsule system were exploited by using path-following (continuation) methods for non-smooth delay differential equations.

Our numerical studies revealed that the DFC with a constant delay can reach the period-1 response from the period-3 response for all the control gains K providing that they are sufficiently large. For a certain range of control gain, the controlled system can converge to the desired motion rapidly with only a relatively small energy expenditure. Thus, under this control scenario, maintaining the control parameter K at a lower value in the feasible range may control the system at a desired motion, and can also keep its energy expenditure at a lower level. Our parameter studies also find that the DFC can steer the system towards a period-1 motion for the delays smaller than the excitation period with reasonable control inputs. In addition, numerical continuation analysis for non-smooth dynamical systems with time delays was employed to study more detailed dynamics of the controlled capsule system with a small time delay. When varying the main control parameters, namely the time delay and the control gain, we observed that the DFC stabilised the period-1 motion in a large region of these control parameters. In particular, the feasible range of these parameters was identified between the occurrences of a period-doubling and a grazing bifurcations via two-parameter continuation.

Because the studied system (14) with DFC (15) is piecewise linear in all four regimes, trajectory segments are all known analytically such that one could in principle determine periodic orbits as solutions of exact finite systems of nonlinear algebraic systems of equations. However, determining the linear stability of these periodic orbits requires numerical discretisation of the orbit segments (in our case pseudo-spectral discretisation (23) [51]), which we also use for bifurcation analysis. For all periodic orbits we detected and tracked, our numerical discretisation and event detection methods employ well-studied numerical methods fully within their regime of convergence, such that numerical discretization errors are small compared to the uncertainties of our model. Consequently, all results regarding existence, stability and bifurcations of periodic orbits and the transitions from attractors of the uncontrolled system to periodic orbits when applying DFC are robust with respect to the choice of numerical methods. Our analysis is unable to discover all coexisting attractors of the uncontrolled system, such that our approach cannot guarantee that DFC indeed makes the system globally monostable. However, analysis of basins of attraction as shown in Fig. 3 demonstrates that attractors with large basins are included in our study. The method and analyses discussed in the present work can be applied to study the dynamical systems with a similar structure as the vibro-impact capsule system encountering time delay. The findings of this work can provide guidance for tuning the control parameters of the capsule system in experiment, e.g., [55, 56], which could be the future work of this research project.

Acknowledgements

This work has been supported by EPSRC under Grant No. EP/P023983/1. Dr Zhi Zhang would like to acknowledge the financial support from the University of Exeter for his Exeter International Excellence Scholarship. Prof. Jan Sieber gratefully acknowledges support by EPSRC Fellowship EP/N023544/1 and EPSRC grant EP/V04687X/1.

Compliance with ethical standards

Conflict of interest

The authors declare that they have no conflict of interest concerning the publication of this manuscript.

Data accessibility

The datasets generated and analysed during the current study are available from the corresponding author on reasonable request.

Open access

For the purpose of open access, the author has applied a CC BY public copyright licence to any author accepted manuscript version arising.

References

- [1] Y. Liu, M. Wiercigroch, E. Pavlovskaja, and H. Yu, “Modelling of a vibro-impact capsule system,” *International Journal of Mechanical Sciences*, vol. 66, pp. 2–11, 2013.
- [2] V.-D. Nguyen, K.-C. Woo, and E. Pavlovskaja, “Experimental study and mathematical modelling of a new of vibro-impact moling device,” *International Journal of Non-Linear Mechanics*, vol. 43, no. 6, pp. 542–550, 2008.
- [3] B. Guo, E. Ley, J. Tian, J. Zhang, Y. Liu, and S. Prasad, “Experimental and numerical studies of intestinal frictions for propulsive force optimisation of a vibro-impact capsule system,” *Nonlinear Dynamics*, vol. 101, no. 1, pp. 65–83, 2020.
- [4] Y. Liu, E. Pavlovskaja, M. Wiercigroch, and Z. Peng, “Forward and backward motion control of a vibro-impact capsule system,” *International Journal of Non-Linear Mechanics*, vol. 70, pp. 30–46, 2015.
- [5] J. Páez Chávez, Y. Liu, E. Pavlovskaja, and M. Wiercigroch, “Path-following analysis of the dynamical response of a piecewise-linear capsule system,” *Communications in Nonlinear Science and Numerical Simulation*, vol. 37, pp. 102–114, 2016.
- [6] F. Chernousko, “The optimum rectilinear motion of a two-mass system,” *Journal of applied Mathematics and Mechanics*, vol. 66, no. 1, pp. 1–7, 2002.
- [7] H. Li, K. Furuta, and F. L. Chernousko, “Motion generation of the capsbot using internal force and static friction,” in *Proceedings of the 45th IEEE Conference on Decision and Control*, pp. 6575–6580, IEEE, 2006.
- [8] X. Gu and Z. Deng, “Dynamical analysis of vibro-impact capsule system with hertzian contact model and random perturbation excitations,” *Nonlinear Dynamics*, vol. 92, no. 4, pp. 1781–1789, 2018.
- [9] H. Zhao and H. Ouyang, “A capsule-structured triboelectric energy harvester with stick-slip vibration and vibro-impact,” *Energy*, vol. 235, p. 121393, 2021.

- [10] Y. Zhang and G. Luo, “Multistability of a three-degree-of-freedom vibro-impact system,” *Communications in Nonlinear Science and Numerical Simulation*, vol. 57, pp. 331–341, 2018.
- [11] H. Xu and J. Ji, “Analytical-numerical studies on the stability and bifurcations of periodic motion in the vibro-impact systems with clearances,” *International Journal of Non-Linear Mechanics*, vol. 109, pp. 155–165, 2019.
- [12] E. Pavlovskaja, D. C. Hendry, and M. Wiercigroch, “Modelling of high frequency vibro-impact drilling,” *International Journal of Mechanical Sciences*, vol. 91, pp. 110–119, 2015.
- [13] L. Serdukova, R. Kuske, and D. Yurchenko, “Post-grazing dynamics of a vibro-impacting energy generator,” *J. Sound Vib.*, vol. 492, p. 115811, 2021.
- [14] K. Mora, A. R. Champneys, A. D. Shaw, and M. I. Friswell, “Explanation of the onset of bouncing cycles in isotropic rotor dynamics; a grazing bifurcation analysis,” *Proc. R. Soc. A*, vol. 476, p. 20190549, 2020.
- [15] Y. Liu, J. Páez Chávez, D. S. Rulston, and S. Walker, “Numerical and experimental studies of stick-slip oscillations in drill-strings,” *Nonlinear Dynamics*, vol. 90, pp. 2959–2978, 2017.
- [16] O. Makarenkov and J. S. W. Lamb, “Dynamics and bifurcations of nonsmooth systems: a survey,” *Physica D*, vol. 241, pp. 1826–1844, 2012.
- [17] A. N. Pisarchik and U. Feudel, “Control of multistability,” *Physics Reports*, vol. 540, no. 4, pp. 167–218, 2014.
- [18] E. Ott, C. Grebogi, and J. A. Yorke, “Controlling chaos,” *Physical review letters*, vol. 64, no. 11, p. 1196, 1990.
- [19] Y.-C. Lai and T. Tél, *Transient chaos: complex dynamics on finite time scales*, vol. 173. Springer Science & Business Media, 2011.
- [20] H. Hu, “Controlling chaos of a periodically forced nonsmooth mechanical system,” *Acta Mechanica Sinica*, vol. 11, no. 3, pp. 251–258, 1995.
- [21] M. Kleczka, E. Kreuzer, and W. Schiehlen, “Local and global stability of a piecewise linear oscillator,” *Philosophical Transactions of the Royal Society of London. Series A: Physical and Engineering Sciences*, vol. 338, no. 1651, pp. 533–546, 1992.
- [22] S. L. de Souza and I. L. Caldas, “Controlling chaotic orbits in mechanical systems with impacts,” *Chaos, Solitons & Fractals*, vol. 19, no. 1, pp. 171–178, 2004.
- [23] C. Begley and L. Virgin, “On the ogy control of an impact-friction oscillator,” *Journal of Vibration and Control*, vol. 7, no. 6, pp. 923–931, 2001.
- [24] J. Ji and A. Leung, “Bifurcation control of a parametrically excited duffing system,” *Nonlinear Dynamics*, vol. 27, no. 4, pp. 411–417, 2002.
- [25] J. Ji, “Local bifurcation control of a forced single-degree-of-freedom nonlinear system: saddle-node bifurcation,” *Nonlinear Dynamics*, vol. 25, no. 4, pp. 369–382, 2001.
- [26] Y. Liu and J. Páez Chávez, “Controlling coexisting attractors of an impacting system via linear augmentation,” *Physica D: Nonlinear Phenomena*, vol. 348, pp. 1–11, 2017.
- [27] Z. Zhang, J. Páez Chávez, J. Sieber, and Y. Liu, “Controlling coexisting attractors of a class of non-autonomous dynamical systems,” *Physica D: Nonlinear Phenomena*, vol. 431, p. 133134, 2022.
- [28] L.-Z. Wang, R.-Q. Su, Z.-G. Huang, X. Wang, W.-X. Wang, C. Grebogi, and Y.-C. Lai, “A geometrical approach to control and controllability of nonlinear dynamical networks,” *Nature communications*, vol. 7, no. 1, pp. 1–11, 2016.

- [29] S. P. Cornelius, W. L. Kath, and A. E. Motter, “Realistic control of network dynamics,” *Nature communications*, vol. 4, no. 1, pp. 1–9, 2013.
- [30] Z. Zhang, J. Páez Chávez, J. Sieber, and Y. Liu, “Controlling grazing-induced multistability in a piecewise-smooth impacting system via the time-delayed feedback control,” *Nonlinear Dynamics*, pp. 1–16, 2021.
- [31] K. Pyragas, “Continuous control of chaos by self-controlling feedback,” *Physics letters A*, vol. 170, no. 6, pp. 421–428, 1992.
- [32] Y. Liu and J. Páez Chávez, “Controlling multistability in a vibro-impact capsule system,” *Nonlinear Dynamics*, vol. 88, pp. 1289–1304, 2017.
- [33] J. Xue, S. Zhang, and J. Xu, “Coordinated optimization of locomotion velocity and energy consumption in vibration-driven system,” *Meccanica*, pp. 1–15, 2022.
- [34] E. Tkachenko, D. Merkulov, D. Pelevina, V. Turkov, A. Vinogradova, and V. Naletova, “Mathematical model of a mobile robot with a magnetizable material in a uniform alternating magnetic field,” *Meccanica*, pp. 1–13, 2022.
- [35] S. Dulin, K. Lin, L. Serdukova, R. Kuske, and D. Yurchenko, “Improving the performance of a two-sided vibro-impact energy harvester with asymmetric restitution coefficients,” *International Journal of Mechanical Sciences*, vol. 217, p. 106983, 2022.
- [36] S. K. Gupta, J. Wang, and O. R. Barry, “Nonlinear vibration analysis in precision motion stage with pid and time-delayed feedback controls,” *Nonlinear Dynamics*, vol. 101, no. 1, pp. 439–464, 2020.
- [37] S. Sudharsan, A. Venkatesan, P. Muruganandam, and M. Senthilvelan, “Suppression of extreme events and chaos in a velocity-dependent potential system with time-delay feedback,” *Chaos, Solitons & Fractals*, vol. 161, p. 112321, 2022.
- [38] Y. Zheng and J. Yu, “Stabilization of multi-rotation unstable periodic orbits through dynamic extended delayed feedback control,” *Chaos, Solitons & Fractals*, vol. 161, p. 112362, 2022.
- [39] D. S. Naidu, *Optimal control systems*. CRC press, 2002.
- [40] M. Franchek, M. Ryan, and R. Bernhard, “Adaptive passive vibration control,” *Journal of Sound and Vibration*, vol. 189, no. 5, pp. 565–585, 1996.
- [41] Y. Liu, T. Waters, and M. Brennan, “A comparison of semi-active damping control strategies for vibration isolation of harmonic disturbances,” *Journal of sound and vibration*, vol. 280, no. 1-2, pp. 21–39, 2005.
- [42] Z. Zhang, Y. Liu, and J. Sieber, “Calculating the lyapunov exponents of a piecewise-smooth soft impacting system with a time-delayed feedback controller,” *Communications in Nonlinear Science and Numerical Simulation*, vol. 91, p. 105451, 2020.
- [43] K. Engelborghs, T. Luzyanina, and D. Roose, “Numerical bifurcation analysis of delay differential equations using dde-biftool,” *ACM Transactions on Mathematical Software (TOMS)*, vol. 28, no. 1, pp. 1–21, 2002.
- [44] J. Sieber, K. Engelborghs, T. Luzyanina, G. Samaey, and D. Roose, *DDE-BIFTOOL Manual-Bifurcation analysis of delay differential equations*, 2017. Available at <http://sourceforge.net/projects/ddebiftool>.
- [45] R. Szalai, G. Stépán, and S. John Hogan, “Continuation of bifurcations in periodic delay-differential equations using characteristic matrices,” *SIAM Journal on Scientific Computing*, vol. 28, no. 4, pp. 1301–1317, 2006.

- [46] R. Szalai, *Knut: a continuation and bifurcation software for delay-differential equations*. Department of Engineering Mathematics, University of Bristol, 2013. Available at <http://rs1909.github.io/knut>.
- [47] J. Páez Chávez, Z. Zhang, and Y. Liu, “A numerical approach for the bifurcation analysis of non-smooth delay equations,” *Commun. Nonlinear Sci. Numer. Simul.*, vol. 83, p. 105095, 2020. (16 pages).
- [48] G. S. Mfoumou, G. D. Kenmoé, and T. Kofané, “Computational algorithms of time series for stick-slip dynamics and time-delayed feedback control of chaos for a class of discontinuous friction systems,” *Mechanical systems and signal processing*, vol. 119, pp. 399–419, 2019.
- [49] I. M. Repin, “On the approximate replacement of systems with lag by ordinary dynamical systems,” *J. Appl. Math. Mech.*, vol. 29, no. 2, pp. 254–264, 1965.
- [50] P. Thota and H. Dankowicz, “Tc-hat (tc): a novel toolbox for the continuation of periodic trajectories in hybrid dynamical systems,” *SIAM Journal on Applied Dynamical Systems*, vol. 7, no. 4, pp. 1283–1322, 2008.
- [51] D. Breda, O. Diekmann, M. Gyllenberg, F. Scarabel, and R. Vermiglio, “Pseudospectral discretization of nonlinear delay equations: new prospects for numerical bifurcation analysis,” *SIAM Journal on applied dynamical systems*, vol. 15, no. 1, pp. 1–23, 2016.
- [52] H. Dankowicz and F. Schilder, *Recipes for continuation*. Computational Science and Engineering, Philadelphia: SIAM, 2013.
- [53] L. F. Shampine and S. Thompson, “Event location for ordinary differential equations,” *Comput. Math. Appl.*, vol. 39, no. 5-6, pp. 43–54, 2000.
- [54] L. F. Shampine and S. Thompson, “Solving DDEs in MATLAB,” *Appl. Numer. Math.*, vol. 37, no. 4, pp. 441–458, 2001.
- [55] B. Guo, Y. Liu, R. Birler, and S. Prasad, “Self-propelled capsule endoscopy for small-bowel examination: Proof-of-concept and model verification,” *International Journal of Mechanical Sciences*, vol. 174, p. 105506, 2020.
- [56] Y. Liu, E. Pavlovskaja, and M. Wiercigroch, “Experimental verification of the vibro-impact capsule model,” *Nonlinear Dynamics*, vol. 83, no. 1-2, pp. 1029–1041, 2016.